Research Square

Preprints are preliminary reports that have not undergone peer review.
They should not be considered conclusive, used to inform clinical practice,
or referenced by the media as validated information.

Quantum Percolation Pathways in Disordered Semiconductor Nanorod Networks

Tigran A. Sargsian
Institute of Chemical Physics NAS RA

Sargis P. Gavalajyan
Russian-Armenian University

Rodion R. Reznik
Alferov University

Paytsar A. Mantashyan
paytsar.mantashyan@rau.am

Russian-Armenian University

David B. Hayrapetyan
Institute of Chemical Physics NAS RA

Article

Keywords:

Posted Date: November 20th, 2026

DOI: https://doi.org/10.21203/rs.3.rs-11547835/v1

License: This work is licensed under a Creative Commons Attribution 4.0 International License.
Read Full License

Additional Declarations: No competing interests reported.

Quantum Percolation Pathways in Disordered Semiconductor Nanorod Networks

Tigran A. Sargsian[1,↓], Sargis P. Gavalajyan[2,1,3,↓], Rodion R. Reznik[4,5,6], Paytsar A. Mantashyan[1,2,*], and David B. Hayrapetyan[1,2]

[1]A.B. Nalbandyan Institute of Chemical Physics, Quantum Materials and Nanophotonics Laboratory, Yerevan, 0014, Armenia
[2]Russian-Armenian University, Department of General Physics and Quantum Nanostructures, Yerevan, 0051, Armenia
[3]University of Patras, Patras, 26504, Greece
[4]Alferov University, St. Petersburg, 194021, Russia
[5]St. Petersburg State University, St. Petersburg, 199034, Russia
[6]Institute for Analytical Instrumentation RAS, St. Petersburg, 190103, Russia
[*]paytsar.mantashyan@rau.am
[↓]*these authors contributed equally to this work*

Abstract

Charge transport in disordered semiconductor nanostructure networks is governed by both structural morphology and quantum-mechanical coupling between neighboring building blocks. Here, we present an image analysis guided computational framework for identifying tunneling-assisted quantum-percolation pathways in disordered InAs nanorod ensembles. Experimentally reported nanorod dimensions are used to reconstruct statistically realistic networks incorporating variations in size, position, orientation, and local density. Automated image analysis extracts the geometrical descriptors of individual nanorods, which are subsequently combined with finite element electronic structure calculations and Bardeen transfer Hamiltonian analysis to evaluate inter-nanorod tunneling rates. The resulting weighted connectivity graphs are analyzed to identify boundary-spanning quantum percolation pathways.

Representative ensembles containing 28, 35, and 38 nanorods reveal a transition from isolated tunneling clusters to boundary-spanning transport pathways as the nanorod density increases. A complementary geometrical percolation analysis demonstrates that the predicted threshold is highly sensitive to the selected connectivity criterion: increasing the geometrical cutoff from 2 to 6 nm shifts the characteristic critical nanorod number from 48.5 to 26.5, corresponding to a reduction of approximately 45%. These results highlight the limitations of purely distance-based connectivity models and demonstrate that long-range transport pathways are governed by the collective distribution of quantum-mechanical coupling strengths rather than by geometrical proximity alone. The proposed framework provides a versatile approach for linking structural morphology with quantum transport behavior and can be extended to a broad range of disordered nanoscale materials.

1. Introduction

The controlled assembly of nanoscale building blocks into functional mesoscale architectures represents one of the central directions of modern nanoscience and materials engineering[1,2,3,4,5,6]. Semiconductor nanostructures are particularly attractive in this context because their electronic, optical, and transport properties can be tuned through composition, size, shape, and surface chemistry[7]. When individual nanostructures are integrated into dense ensembles, their collective behavior often differs substantially from

that of isolated particles, giving rise to emergent phenomena that are inaccessible at the single-particle level[3,4,5,6]. Such effects have created broad opportunities for next-generation optoelectronic devices, photovoltaics, photodetectors, and chemical or biological sensing platforms.

Among semiconductor nanostructures, nanorods stand out because of their elongated geometry and the resulting anisotropic confinement of charge carriers.[8,9,10,11] Unlike nearly spherical quantum dots, their electronic coupling, optical response, and emission polarization depend strongly on nanorod orientation[11,12]. Advances in nanorod fabrication have enabled precise control over their length, diameter, aspect ratio, composition, and surface properties, providing considerable flexibility for tailoring their physical behavior. Semiconductor nanorods have therefore attracted interest for a broad range of applications, including light-emitting devices, photovoltaics, photodetectors, optical and chemical sensors, and nanoscale electronic and optoelectronic systems.

When nanorods are brought into close proximity, their collective behavior becomes governed not only by the properties of individual rods but also by their interactions with neighboring structures. In disordered nanorod assemblies, charge carriers may move through tunneling or hopping between localized states on adjacent nanorods[13,14,15,16,17]. In such disordered systems, the spatially nonuniform arrangement of nanorods produces a broad distribution of interparticle coupling strengths, causing charge transport to develop preferentially along specific sequences of strongly coupled particles and giving rise to dominant transport pathways across the network. These pathways play a central role in determining macroscopic conductivity, carrier mobility, and overall device performance[18,19,20]. Nanorod assemblies are therefore particularly promising as functional building blocks for charge-transport layers and other optoelectronic architectures in which directional electronic or energy transfer is required. Understanding how microscopic nanorod morphology controls the formation of such pathways remains an important problem in nanostructured materials.

This problem is not unique to nanorod systems, but is part of a broader class of disordered materials, such as amorphous semiconductors, granular media, heavily doped systems, and organic electronic materials[21,22,23]. In all these cases, charge transport takes place in complex and irregular energy landscapes shaped by structural disorder and variations in local coupling. As a result, charge carriers do not move uniformly but preferentially propagate through strongly coupled or favorably connected regions, leading to the formation of dominant conduction pathways. While percolation theory has provided important general insights into such behavior, identifying these pathways at the microscopic level in realistic systems remains a challenging task. Moreover, conventional percolation models commonly define connectivity through particle contact or an specified geometrical distance criterion. At the nanoscale, however, geometrical proximity alone does not necessarily provide a direct measure of electronic connectivity, which is governed by the quantum-mechanical coupling between localized states.

Semiconductor nanorod assemblies offer a particularly useful platform for studying this problem, as they combine experimentally accessible structures with tunable quantum interactions. However, a key difficulty is establishing a direct link between the actual arrangement of nanorods observed in experiments and the resulting charge transport properties. Many existing models rely on simplified or idealized structures that do not fully reflect the complexity of real systems, where disorder in position, orientation, size, and spacing plays a crucial role. At the same time, direct quantum-mechanical treatment of large disordered ensembles can become computationally demanding. A framework capable of translating complex nanorod morphology into a physically weighted transport network is therefore needed to bridge structural reconstruction and quantum-mechanical transport analysis.

In this work, we address this challenge by introducing an image-analysis-guided framework for identifying quantum percolation pathways in disordered nanorod networks. Automated image-processing techniques[24,25] are used to convert microscopy-like images into quantitative geometrical datasets containing the positions, sizes, and orientations of individual nanorods. The electronic states of individual nanorods

are then calculated by solving the Schrödinger equation within the effective-mass approximation using the finite element method[16,26]. Tunneling rates between neighboring nanorods are evaluated using Bardeen's transfer Hamiltonian approach[27,28] and subsequently used to construct a weighted network describing the system. This image-to-physics workflow enables the influence of nanorod density, structural disorder, orientation, and local electronic coupling on the emergence of transport pathways to be examined directly. More broadly, it provides a transferable framework for connecting structural morphology with quantum transport behavior in disordered nanoscale systems.

2. Materials and Methods

2.1. Reconstruction of Nanorod Geometry and Extraction of Structural Parameters

In the present work, disordered ensembles of indium arsenide (*InAs*) semiconductor nanorods are considered as a model platform for investigating tunneling induced quantum transport in nanostructured networks. *InAs* was selected because of its narrow bandgap and small electron effective mass[29], which favor strong quantum confinement while allowing appreciable wavefunction penetration into the surrounding barrier region. Consequently, electronic coupling through tunneling can remain significant between neighboring nanorods, making *InAs* nanorod ensembles a suitable model system for investigating quantum-percolation effects.

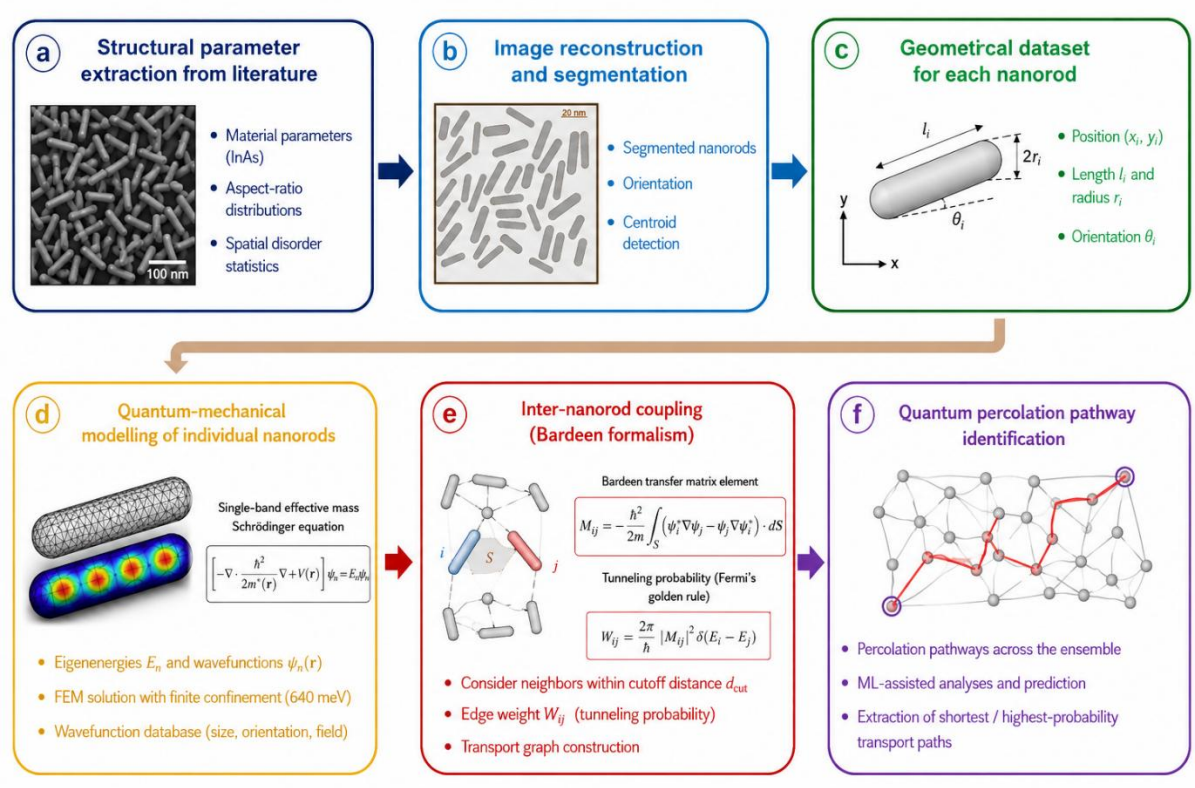


Figure 1. Image analysis guided framework for identifying quantum percolation pathways in disordered semiconductor nanorod networks. (a) Definition of the nanorod size and aspect-ratio ranges using experimentally reported structural characteristics. (b) Generation of disordered synthetic nanorod ensembles and corresponding microscopy-like images. (c) Automated image processing and extraction of the geometrical dataset containing the position, dimensions, and orientation of each nanorod. (d) Finite element calculation of localized electronic states for individual nanorods. (e) Evaluation of pairwise wavefunction overlap based coupling and construction of the weighted connectivity graph. (f) Identification of boundary-spanning percolation pathways within the reconstructed network.

To ensure that the reconstructed ensembles remain representative of experimentally realizable nanorod systems, the geometrical parameters were selected based on experimentally reported dimensions of synthesized InAs nanorods[29]. In particular, the size and aspect-ratio ranges used in the simulations were chosen to reproduce experimentally relevant nanorod geometries. Although the geometrical parameters adopted here are based on nanorods produced by colloidal synthesis, the computational framework itself is independent of the specific fabrication method and can be applied to nanorod ensembles produced by other synthesis or fabrication routes, provided that the corresponding structural and material parameters are supplied. Unlike many previous studies employing idealized lattice models, the present approach reconstructs statistically realistic nanorod ensembles (Fig. 1a) exhibiting positional disorder, orientational dispersion, size fluctuations, and local density variations similar to those observed experimentally.

The synthetic ensembles were generated within a 128x128 nm^2 computational domain (Fig. 1b). Nanorod lengths were sampled over approximately 20–35 nm and radii over approximately 3–4.5 nm, corresponding to diameters of approximately 6–9 nm. The rods were assigned random positions and orientations under a non-overlap constraint. Placement was repeated until either the prescribed number of nanorods or the maximum number of placement attempts was reached. Each nanorod was modeled as a capsule like structure composed of a central rectangular segment terminated by two semicircular caps (Fig. 1c). The geometry of an individual i^{th} nanorod was defined by its length l_i, radius r_i, orientation angle θ_i, and spatial coordinates x_i, y_i.

To reproduce the microscopy-like appearance required for the image-processing workflow, synthetic grayscale images were generated from the reconstructed ensembles by introducing edge enhancement, background texture, and controlled noise (Fig. 1b). These artificial micrographs were used exclusively for visualization and image-processing purposes and do not represent experimentally recorded SEM or TEM images.

Automated image analysis based on connected component labeling was used to identify individual nanorods and extract their geometrical descriptors, including center coordinates, projected dimensions, and orientation angles. The resulting structural dataset was subsequently used as input for the quantum-mechanical calculations. To reduce the computational cost associated with evaluating electronic coupling across all possible nanorod pairs, a preliminary geometrical screening was introduced. Pairs with a center-to-center separation below 50 nm were retained as candidates for subsequent coupling calculations. This distance criterion served exclusively as a computational preselection step, excluding widely separated nanorods for which electronic coupling is expected to be negligible. The connectivity and weighting of the final transport network were then determined from the calculated electronic coupling between the retained nanorod pairs, as described in Sections 2.2 and 2.3.

2.2. Quantum Mechanical Modeling of Electronic States and Inter Nanorod Coupling

The geometrical dataset obtained in Section 2.1 serves as the input for further calculations illustrated in Fig. 1d–f. The electronic states of individual semiconductor nanorods were calculated within the single band effective mass approximation[16,17,26]. Within this framework, charge carriers are treated as quasiparticles confined inside finite semiconductor potentials, and their stationary states are obtained by solving the time-independent Schrödinger equation:

$$\left[-\frac{\hbar^2}{2m^*}\nabla^2 + V(\vec{r})\right]\psi_n(\vec{r}) = E_n\psi_n(\vec{r}) \qquad [1]$$

where m^* is the effective carrier mass, $V(\vec{r})$ - confinement potential defining the nanorod geometry, and $\psi_n(\vec{r})$, E_n are the corresponding eigenfunctions and eigenenergies. The electron effective mass was taken

as 0.023m_0 inside the *InAs* nanorods and 0.067 m_0 in the surrounding barrier material, while a finite confinement barrier of 640 meV was assumed outside the nanorods. The Schrödinger equation was solved numerically using FEM[26], which provides accurate treatment of irregular nanorod geometries and complex computational domains (Fig. 1d).

Because solving the eigenvalue problem for every nanorod within large disordered ensembles is computationally demanding, a database of precomputed wavefunctions was generated for representative combinations of nanorod length, radius, orientation, and applied electric field. During the reconstruction of each ensemble, every nanorod was assigned the wavefunction corresponding to the closest geometrical parameters, followed by the appropriate rotational and translational transformations. This strategy significantly reduces the computational cost while preserving the dependence of the electronic states on the local nanorod geometry.

The reconstructed ensemble-scale wavefunction distributions were subsequently used to evaluate electronic localization and tunneling coupling between neighboring nanorods (Fig. 1e). Charge transport within disordered nanorod ensembles was assumed to occur predominantly through quantum tunneling between neighboring localized states. In weakly coupled nanostructures, electronic wavefunctions remain largely confined inside individual nanorods while exhibiting finite penetration into the surrounding barrier region. As a consequence, transport is governed by wavefunction overlap between adjacent nanorods rather than by fully delocalized band-like motion.

Thus, electronic transport between nanorods was described using Bardeen's transfer Hamiltonian formalism[31,32]. Within this approach, neighboring nanorods are treated as weakly interacting subsystems described by localized eigenstates ψ_i, ψ_j, while tunneling transitions are induced through a perturbative transfer Hamiltonian:

$$H = H_i + H_j + H_T \quad [2]$$

where H_i and H_j describe the isolated electronic states of neighboring nanorods and H_T denotes the transfer Hamiltonian responsible for tunneling transitions between them. The tunneling transition rate between initial and final states was evaluated using Fermi's golden rule:

$$W_{ij} = 2\pi/\hbar \left|M_{ij}\right|^2 \delta\left(E_i - E_j\right) \quad [3]$$

where E_i and E_j are the energies of the initial and final states, respectively, and M_{ij} is the transfer matrix element describing the tunneling interaction across the barrier region. The transfer matrix element was calculated according to Bardeen's formulation,

$$M_{ij} = \frac{\hbar^2}{2m^*} \int_S \left(\psi_i^* \nabla \psi_j - \psi_j \nabla \psi_i^*\right) \cdot d\vec{S} \quad [4]$$

where the integration surface $d\vec{S}$ is chosen inside the barrier region separating neighboring nanorods. Only elastic tunneling processes were considered in the present work by assuming a time-independent transfer Hamiltonian.

2.3. Construction of the Quantum Percolation Network

The tunneling rates obtained from Bardeen's transfer Hamiltonian were used to construct a weighted graph representing the quantum transport network of the nanorod ensemble (Fig. 1e). Each nanorod was

represented as a graph node, while every tunneling event between neighboring nanorods was represented by an edge weighted according to the corresponding tunneling rates W_{ij}. Consequently, the resulting graph simultaneously incorporates the structural morphology of the ensemble and the quantum mechanical coupling between neighboring nanorods. Thus, the geometrical search distance serves only as a computational preselection criterion for candidate nanorod pairs, whereas the existence and weight of connections in the final transport network are determined by the calculated quantum-mechanical tunneling coupling.

The weighted graph was subsequently analyzed to identify continuous percolation pathways spanning the reconstructed nanorod ensemble. Unlike conventional geometrical percolation models, in which connectivity is determined solely by particle contact or a prescribed distance criterion, the present approach determines the connectivity of candidate nanorod pairs from their calculated quantum-mechanical tunneling coupling. Consequently, the identified percolation pathways (Fig. 1f) represent the most favorable routes for carrier transport through disordered nanorod networks and establish a direct computational link between structural morphology and quantum transport behavior.

3. Results and Discussion

3.1. Formation of Quantum Percolation Pathways in Disordered Nanorod Networks

The formation of continuous charge transport pathways in disordered semiconductor nanorod ensembles is governed by the interplay between structural morphology and quantum mechanical coupling between neighboring nanorods. To investigate this relationship, three representative ensembles containing 28, 35, and 38 nanorods were analyzed within the same computational domain. Fig. 2 presents the reconstructed nanorod morphologies, the corresponding electron probability density distributions obtained from the finite element calculations, and the resulting tunneling-assisted transport networks. Although the increase in nanorod density is relatively modest, the transport behavior changes qualitatively, revealing the transition from isolated tunneling clusters to a continuous quantum percolation pathway.

The physical origin of this behavior is evident from the calculated electron probability density distributions shown in the second row of Fig. 2. In all cases, the electronic states remain strongly localized within individual nanorods due to quantum confinement, while simultaneously extending into the surrounding barrier through exponentially decaying evanescent tails. Although these tails penetrate only a short distance into the barrier, they enable electronic coupling between neighboring nanorods. Consequently, relatively small reductions in interparticle separation can produce substantial increases in the tunneling rate calculated using Bardeen's transfer Hamiltonian formalism. As the nanorod density increases, the ensemble evolves from a collection of weakly interacting quantum objects into an interconnected quantum network capable of supporting long-range carrier transport.

This evolution is directly reflected in the calculated transport networks shown in the third row of Fig. 2. For the ensemble containing 28 nanorods, electronic coupling is limited to several disconnected regions. Although local tunneling occurs between neighboring nanorods, these isolated tunneling clusters do not merge into a continuous pathway spanning the system. Consequently, no continuous transport pathway spans the computational domain, indicating that the ensemble remains below the quantum-percolation threshold.

A qualitative transition is observed when the number of nanorods increases to 35. The reduced average spacing enhances the electronic coupling sufficiently to connect previously isolated tunneling clusters, resulting in the formation of the first continuous quantum-percolation pathway extending across the ensemble. Notably, the identified pathway does not necessarily coincide with the shortest geometrical route across the computational domain. Instead, it follows a sequence of nanorods characterized by

favorable tunneling coupling, demonstrating that long-range charge transport is governed by the collective distribution of quantum-mechanical coupling strengths rather than by geometrical proximity alone.

For the ensemble containing 38 nanorods, the transport network becomes considerably more robust. The larger number of neighboring tunneling connections creates multiple alternative conductive branches, reducing the dependence of the spanning network on individual weak links and producing a more highly connected and redundant percolation network. In this regime, charge transport is supported by a highly interconnected tunneling network rather than by only a few critical tunneling events, indicating that the system has evolved well beyond the onset of quantum percolation.

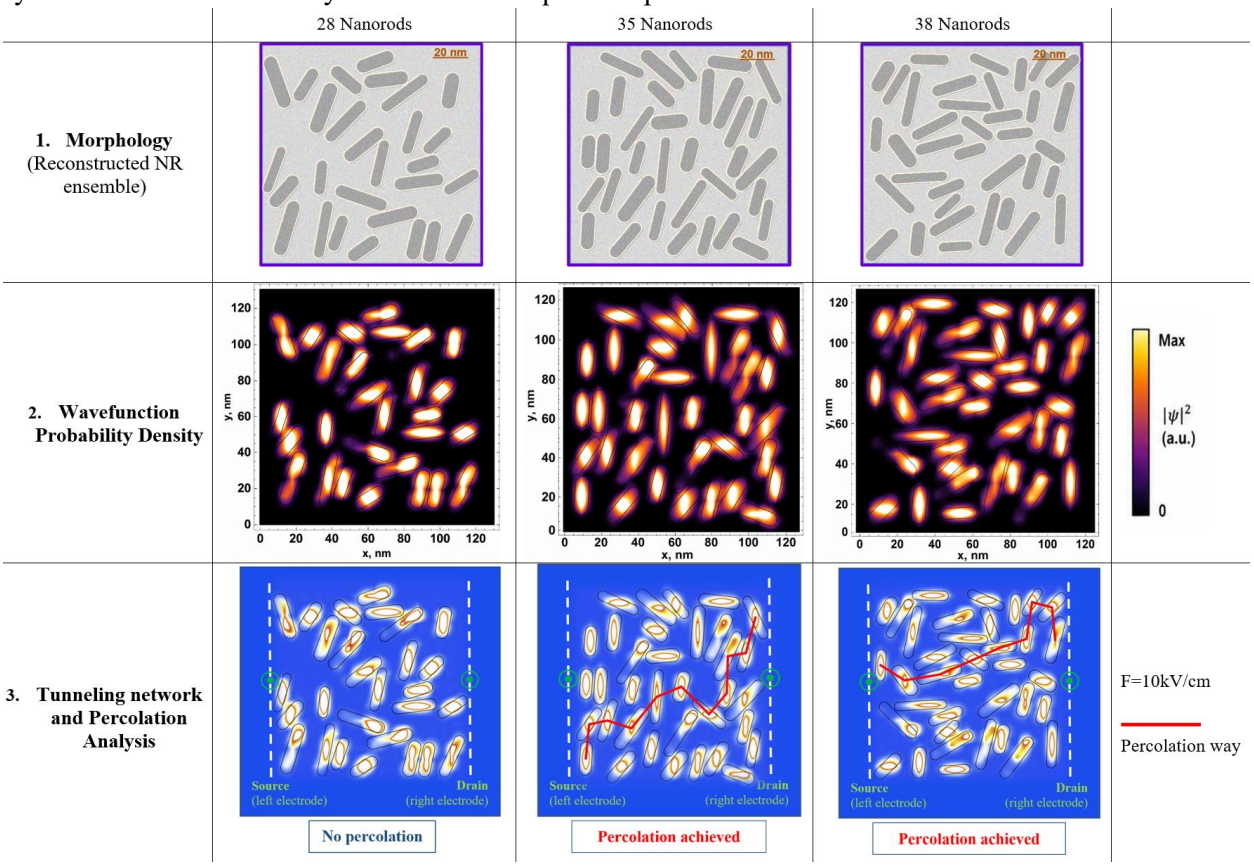


Figure 2. Figure 2. Identification of quantum-percolation pathways in reconstructed semiconductor nanorod ensembles. Representative networks containing 28, 35, and 38 nanorods are shown together with their corresponding electron probability density distributions and tunneling-assisted transport pathways. The identified percolation pathways (bold red lines) reveal the transition from localized tunneling clusters to a boundary-spanning transport network as the nanorod density increases.

These results demonstrate that the transition from disconnected tunneling clusters to a boundary-spanning transport network is not simply a consequence of increasing nanorod density. Rather, it reflects the collective evolution of quantum-mechanical coupling throughout the ensemble. While increasing the number of nanorods increases the number of potential tunneling events, a continuous transport pathway is established only when the tunneling rates become sufficiently large to connect previously isolated clusters. The observed transition therefore represents a quantum-percolation process in which the formation of long-range transport pathways is determined jointly by structural disorder and electronic coupling between neighboring localized states.

3.2. Quantitative Analysis of Quantum Percolation

While the representative ensembles in Fig. 2 illustrate the emergence of quantum-percolation pathways, it is instructive to first examine how the predicted percolation threshold depends on a purely geometrical definition of connectivity. For this purpose, a conventional geometrical percolation analysis was performed in which two nanorods were considered connected when their edge-to-edge separation was smaller than a prescribed cutoff distance. Figure 3 shows the resulting percolation probability as a function of nanorod number for cutoff distances of 2, 4 and 6 nm. In all cases, the calculated probabilities are well described by logistic functions, allowing the corresponding characteristic percolation thresholds to be estimated.

A clear systematic trend is observed as the cutoff distance increases. For a 2 nm cutoff the probability of forming a continuous network remains very low throughout the investigated density range and reaches only about 30% for the largest ensemble containing 46 nanorods. The corresponding critical nanorod number, obtained from the logistic fit, is N_c=48.5, indicating that the system remains below the percolation threshold under such a restrictive connectivity criterion.

When the cutoff distance is increased to 4 nm, the behavior changes markedly. The percolation probability rises rapidly from nearly zero to almost unity over a relatively narrow density range, with the transition centered at N_c =34.6. Increasing the cutoff further to 6 nm shifts the transition to even lower nanorod number, yielding a critical value of N_c =26.5. In this case, a continuous transport pathway is established even for comparatively sparse ensembles.

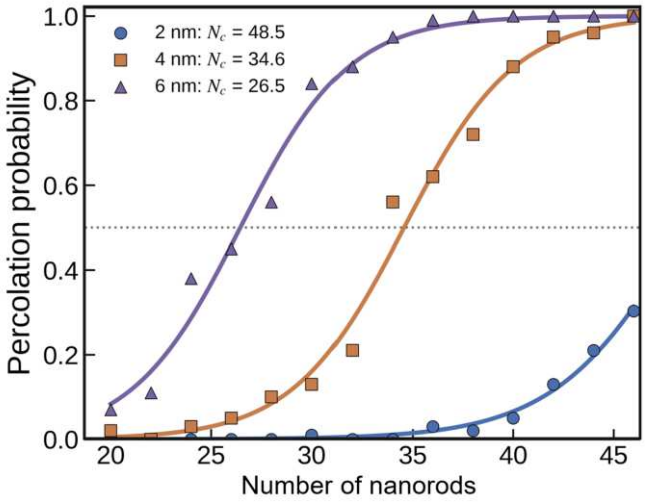


Figure 3. Percolation probability as a function of nanorod number for different geometrical connectivity cutoffs. Solid curves represent logistic fits used to estimate the corresponding critical nanorod numbers.

Overall, increasing the cutoff distance from 2 to 6 nm reduces the predicted critical nanorod number by almost 45%. This pronounced shift demonstrates that the percolation threshold obtained from conventional geometrical models is highly sensitive to the selected connectivity criterion. Because the cutoff distance is an externally imposed model parameter rather than an independently determined physical connectivity criterion, different choices can lead to substantially different predictions for the onset of percolation.

In contrast, the framework proposed in this work constructs the transport network using quantum-mechanical tunneling rates calculated within Bardeen's transfer Hamiltonian formalism. Following the preliminary geometrical selection of candidate nanorod pairs described in Section 2.1, the connectivity and weight of the corresponding network edges are determined by the strength of their electronic coupling rather

than solely by an arbitrarily selected geometrical cutoff. Consequently, nanorods with similar edge-to-edge separations may contribute very differently to the transport network because of differences in wavefunction overlap and the resulting tunneling rates.

Taken together, the quantum-network analysis in Fig. 2 and the geometrical comparison in Fig. 3 demonstrate the importance of going beyond particle density and simple distance-based connectivity criteria when describing long-range transport in disordered nanorod networks. Although the morphology defines the set of potentially interacting nanorods, a boundary-spanning quantum transport pathway emerges only when the distribution of electronic coupling strengths is sufficient to connect localized states across the ensemble.

An important advantage of the proposed framework is its ability to establish a quantitative connection between nanostructure morphology and quantum transport characteristics. In the present study, this capability is demonstrated using statistically reconstructed nanorod ensembles and corresponding synthetic microscopy-like images. The image-analysis workflow converts these structures into quantitative geometrical datasets, which are subsequently combined with finite element electronic-structure calculations and quantum-tunneling analysis to identify the dominant percolation pathways. The same workflow can, in principle, be applied to experimentally acquired microscopy images, allowing measured structural information to serve directly as input for quantum-transport analysis. Owing to its modular design, the framework can be extended to a broad range of disordered nanostructured materials, including semiconductor nanorod films, quantum-dot solids, nanowire assemblies, and other systems in which carrier transport is governed by tunneling or hopping between nanoscale building blocks.

Conclusions

In this work, we introduced an image analysis guided computational framework for identifying quantum-percolation pathways in disordered semiconductor nanorod networks. By combining statistically realistic morphology reconstruction, automated extraction of geometrical descriptors, finite element electronic-structure calculations, and Bardeen transfer Hamiltonian analysis, the proposed approach establishes a direct computational link between nanorod morphology and the resulting quantum transport network.

The results demonstrate that increasing the nanorod density drives a transition from isolated tunneling clusters to boundary-spanning transport pathways. Importantly, this transition cannot be described by geometrical proximity alone. Instead, the emergence of long-range transport pathways is governed by the collective distribution of quantum-mechanical tunneling rates, which depends on both the structural morphology of the ensemble and the electronic coupling between neighboring nanorods.

The geometrical percolation analysis further demonstrates the strong sensitivity of the predicted percolation threshold to the choice of connectivity criterion. Increasing the geometrical cutoff distance from 2 to 6 nm shifts the characteristic critical nanorod number from 48.5 to 26.5, corresponding to a reduction of approximately 45%. This pronounced variation highlights the limitations of describing transport connectivity solely through an externally imposed distance criterion and emphasizes the importance of incorporating quantum-mechanical coupling when analyzing percolation in disordered nanostructured materials.

Beyond the specific *InAs* nanorod system considered here, the proposed framework is not restricted to a particular synthesis or fabrication method and can be extended to a broad class of disordered nanostructured materials, including nanowire assemblies, quantum-dot solids, and other systems in which carrier transport is governed by tunneling or hopping between localized nanoscale building blocks. The image-analysis component also provides a route toward the direct incorporation of experimentally acquired microscopy data into quantum-transport calculations. The methodology therefore offers a versatile

computational approach for linking structural morphology with quantum transport behavior and may contribute to the design and optimization of nanoscale electronic and optoelectronic materials.

Data and code availability

The data and code supporting the findings of this study, including the generated nanorod geometries, extracted geometrical descriptors, tunneling calculations, and network-connectivity analyses, are publicly available in Zenodo at https://zenodo.org/records/22898208.

Competing Interests

The authors declare no competing interests.

Acknowledgements

The work of T.A.S., P.A.M., and D.B.H. was supported by the Science Committee of the Republic of Armenia under Research Project No. 24FP-2A029. The tunneling calculations performed by R.R.R. were supported by Saint Petersburg State University under Research Project No. 122040800254-4.

Author Contributions

T.A.S. and S.P.G. contributed equally to this work. T.A.S. developed and implemented the image-analysis and network-reconstruction workflow and contributed to data analysis and figure preparation. S.P.G. contributed to the theoretical model, numerical calculations, analysis of the electronic states, and interpretation of the transport pathways. R.R.R. contributed to the selection and interpretation of experimentally relevant nanorod parameters and reviewed the manuscript. P.A.M. contributed to the conception of the study, methodology, project coordination, interpretation of the results, and writing and revision of the manuscript. D.B.H. contributed to the theoretical framework, supervision, interpretation of the results, and revision of the manuscript. All authors reviewed and approved the final manuscript.

References

1. Saran, Rinku, and Richard J. Curry. "Lead sulphide nanocrystal photodetector technologies." Nature Photonics 10.2 (2016): 81-92.
2. Notot, Vincent, et al. "Quantum dot acceptors in two-dimensional epitaxially fused PbSe quantum dot superlattices." ACS nano 16.2 (2022): 3081-3091.
3. Meng, Lingju, et al. "Colloidal quantum dot materials for next-generation near-infrared optoelectronics." Chemical Communications 60.9 (2024): 1072-1088.
4. Xiang, Wuchen, et al. "Surface-deprotonated ultra-small SnO 2 quantum dots for high-performance perovskite solar cells." Energy & Environmental Science 18.1 (2025): 406-417.
5. Chistyakov, A. A., et al. "Optoelectronic properties of semiconductor quantum dot solids for photovoltaic applications." J. Phys. Chem. Lett. 8.17 (2017): 4129-4139.
6. Grotevent, Matthias J., et al. "Temperature-dependent charge carrier transfer in colloidal quantum dot/graphene infrared photodetectors." ACS applied materials & interfaces 13.1 (2020): 848-856.
7. Bimberg, D. ed., 2008. Semiconductor nanostructures. Springer Science & Business Media.
8. Kudera, S., Carbone, L., Casula, M.F., Cingolani, R., Falqui, A., Snoeck, E., Parak, W.J. and Manna, L., 2005. Selective growth of PbSe on one or both tips of colloidal semiconductor nanorods. Nano Letters, 5(3), pp.445-449.

9. Krahne, R., Manna, L., Morello, G., Figuerola, A., George, C. and Deka, S., 2013. Physical properties of nanorods (p. 217). New York: Springer.
10. Sitt, A., Hadar, I. and Banin, U., 2013. Band-gap engineering, optoelectronic properties and applications of colloidal heterostructured semiconductor nanorods. Nano Today, 8(5), pp.494-513.
11. Wang, F., Dong, A. and Buhro, W.E., 2016. Solution–liquid–solid synthesis, properties, and applications of one-dimensional colloidal semiconductor nanorods and nanowires. Chemical reviews, 116(18), pp.10888-10933.
12. Jang, Hyejeong, et al. "Polarized emission from unidirectionally oriented semiconductor nanorods in light-emitting devices." Applied Surface Science 614 (2023): 156160.
13. Zhang, Wanlong, et al. "Optically addressable photoaligned semiconductor nanorods in thin liquid crystal films for display applications." Advanced Optical Materials 6.16 (2018): 1800250.
14. Balberg, I., et al. "Fundamental transport processes in ensembles of silicon quantum dots." Phys. Rev. B 75.23 (2007): 235329.
15. Balberg, I. "Electrical transport in ensembles of semiconductor quantum dots." Physica E: Low-dimensional Systems and Nanostructures 51 (2013): 2-9.
16. Mantashian, G. A., D. B. Hayrapetyan, and P. A. Mantashyan. "Voxel-scale quantum state control in nanorod ensembles using reconfigurable needle beams." Journal of Physics: Photonics 8.1 (2026): 015050.
17. Mantashyan, P., Mantashian, G. and Hayrapetyan, D., 2023. Talbot effect in InAs/GaAs coupled cylindrical quantum dots ensemble. Physica E: Low-dimensional Systems and Nanostructures, 148, p.115662.
18. Zheng, Xiaoyu, et al. "A strategy for dimensional percolation in sheared nanorod dispersions." Advanced Materials 19.22 (2007): 4038-4043.
19. Zhang, Yingjie, et al. "Charge percolation pathways guided by defects in quantum dot solids." Nano letters 15.5 (2015): 3249-3253.
20. Tosheva, Zornitza P., and Jan PF Lagerwall. "Orientational ordering benefits nanorod sonication." Physical Review Materials 10.3 (2026): 035603.
21. Wu, Haoyu, et al. "Manipulating the percolated network of nanorods in polymer matrix by adding non-conductive nanospheres: A molecular dynamics simulation." Composites Science and Technology 229 (2022): 109694.
22. Borghi, F., Mirigliano, M., Dellasega, D. and Milani, P., 2022. Influence of the nanostructure on the electric transport properties of resistive switching cluster-assembled gold films. Applied Surface Science, 582, p.152485.
23. Hazra, S., Dahiya, S., Singh, S.V., Pandey, U., Suman, S., Swaminathan, P. and Pal, B.N., 2024. Flexible transparent conductors with a percolated Ag nanostructure and its application as efficient self-bias plasmonic photodetector. Chemical Engineering Journal, 498, p.155313.
24. Day, A. L., Wahl, C. B., dos Reis, R. et al. Automated image segmentation for accelerated nanoparticle characterization. Scientific Reports 15, 17180 (2025). DOI: 10.1038/s41598-025-01337-z.
25. Baiyasi, R., Gallagher, M.J., McCarthy, L.A., Searles, E.K., Zhang, Q., Link, S. and Landes, C.F., 2020. Quantitative analysis of nanorod aggregation and morphology from Scanning electron micrographs using SEMseg. The Journal of Physical Chemistry A, 124(25), pp.5262-5270.
26. Mantashian, G.A., Mantashyan, P.A. and Hayrapetyan, D.B., 2023. Modeling of quantum dots with the finite element method. Computation, 11(1), p.5.
27. Noguera, C., 1989. Validity of the transfer Hamiltonian approach: application to the STM spectroscopic mode. Journal de Physique, 50(18), pp.2587-2599.

28. Ramprasad, R., Fonseca, L.R.C. and Von Allmen, P., 2000. Calculation of the field-emission current from a surface using the Bardeen transfer Hamiltonian method. Physical Review B, 62(8), p.5216.
29. Kan, Shihai, et al. "Synthesis and size-dependent properties of zinc-blende semiconductor quantum rods." Nature Materials 2.3 (2003): 155-158.
30. Cuadra, L. and Nieto-Borge, J.C., 2021. Modeling quantum dot systems as random geometric graphs with probability amplitude-based weighted links. Nanomaterials, 11(2), p.375.
31. Payne, M.C., 1986. Transfer Hamiltonian description of resonant tunnelling. Journal of Physics C: Solid State Physics, 19(8), pp.1145-1155.
32. Noguera, C., 1989. Validity of the transfer Hamiltonian approach: application to the STM spectroscopic mode. Journal de Physique, 50(18), pp.2587-2599.